9 Chalcopyrite Solar Cells and Modules

R. Klenk

Chalcopyrite-based solar modules are uniquely combining advantages of thin-film technology with the efficiency and stability of conventional crystalline silicon cells. It is therefore believed that chalcopyrite based modules can take up a large part of the PV market growth once true mass production is started. The efficiency of lab-scale thin-film devices is close to 20% [2], an efficiency comparable to the best multicrystalline silicon cells. Many scaling-up and manufacturing issues have been resolved. Pilot production lines are operational and modules are commercially available. As of 2006, the market share of chalcopyrite photovoltaic (PV) modules is not yet significant but major problems that might prevent further commercialization have not been identified.

The first chalcopyrite-based solar cell has been published in 1974 [3]. The cell was prepared from a p-type $CuInSe_2$ (CISe) single crystal onto which a CdS film was evaporated in vacuum. This combination of a p-type chalcopyrite absorber and a wide-gap n-type window layer still is the basic concept upon which current cell designs are based. The typical design, first described in 1985 [4] is shown in Figs. 9.1 and 9.2. The $CuInSe_2$ crystal is replaced by a polycrystalline thin film of the more general composition $Cu(In,Ga)(S,Se)_2$. The thick CdS film is replaced by a very thin, typically 50 nm, CdS film (buffer layer) and a stack of undoped (i-ZnO) and highly doped ZnO (TCO). Cells and modules are prepared in substrate configuration, i.e., the nontransparent metal back contact is the first film to be deposited onto the substrate whereas the transparent ZnO front contact is deposited last.

The requirements for ZnO in chalcopyrite-based photovoltaics are derived from its major functions within the device:

- Formation of the heterojunction
- Lateral current transport
- Passing illumination from the cell surface to the absorber

9.1 Heterojunction Formation

The CdS film used in the first chalcopyrite cell is in some aspects an ideal heterojunction partner for CISe: the conduction bands are reasonably well aligned and the lattice constants match. On the other hand, its relatively low

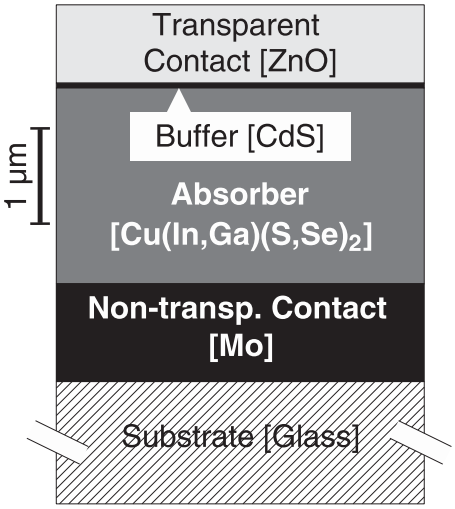

Fig. 9.1. Schematic cross-section of a chalcopyrite-based thin-film solar cell. Typical materials for the individual parts of the cell are given in square brackets

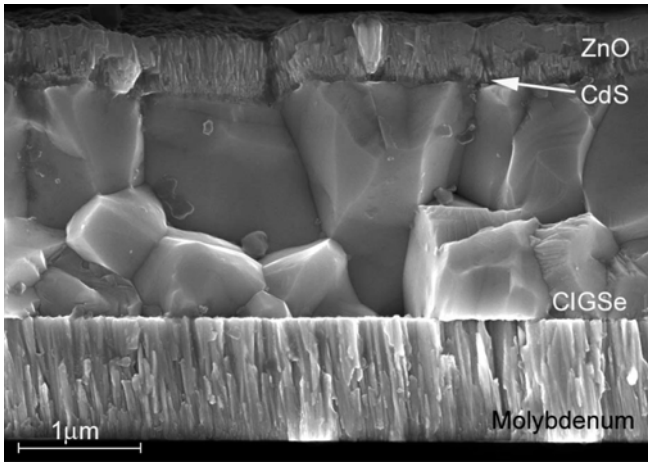

Fig. 9.2. Scanning electron micrograph of the cross-section of a typical chalcopyrite solar cell with $Cu(In,Ga)Se_2$ (CIGSe) absorber (substrate now shown). Reprinted with permission from [1]

band gap ($E_g \approx 2.4\,eV$) causes significant losses in photocurrent and its conductivity is limited. In an effort to improve transparency and conductivity of the window layer without loosing the advantages of CdS concerning junction formation, a very thin CdS film (buffer) was combined with a thick ZnO film [4]. At the same time, the CdS preparation technique was changed from evaporation to chemical bath deposition (CBD). Because of the ideal step

coverage of CBD, the rough absorber surface can be covered completely even by a very thin film. A cross section of an actual device is shown in Fig. 9.2.

It may appear from this description that the ZnO plays a role only in forming an nn-heterojunction, which is not critical in terms of cell performance. However, if the absorber/buffer interface and the buffer itself do not hold sufficient positive electrical charge to balance the space charge region of the absorber, the ZnO properties will influence the Fermi-level position at the pn-junction. It can be shown that this parameter is of crucial importance concerning device performance [5]. In general, the Fermi-level should be close to the conduction band of the absorber at the interface in order to minimise the density of holes available for recombination. Band line-up, buffer doping, and interface charge in chalcopyrite-based heterojunctions are under discussion and may vary depending on materials and preparation techniques. An example for a situation where the TCO does play a role in interface formation is shown in Fig. 9.3a. Here, a different band line-up between buffer and TCO as well as different doping of the TCO would influence the Fermi level position at the absorber/buffer junction and, hence, the performance of the device. There are indications that in most cases the situation is closer to the examples shown in Fig. 9.3c,b, i.e., that the absorber/buffer interface and/or the buffer bulk determine the interface Fermi level. In these cases, a fluctuation in TCO properties will have only a small influence on the interface recombination rate.

Further models for the chalcopyrite-based heterojunction are suggested in literature [6–8]. It is postulated that cadmium diffuses into the absorber surface, converts it to an n-type semiconductor, and causes a buried junction. It is also postulated that this eliminates interface recombination losses due to the spatial separation of the pn-junction and heterojunction. However, calculations reveal that two cases have to be distinguished, none of them necessarily resulting in improved device performance. In the first case, the n-type layer is too shallow or the donor density is too small to equal the charge in the p-type absorber. The surface type conversion will have little influence and the situation is – in principle – still the same as described above and shown in Fig. 9.3a–c. In the second case the n-type layer can hold enough charge, the band diagram will resemble the situation shown in Fig. 9.3d, and the TCO will have little influence on device performance. But the holes photo-generated within the n-type part of the absorber will recombine at the interface to the buffer layer (where they are minority carriers). In analogy to a conventional homojunction solar cell with deep emitter and poorly passivated surface, this reduces the blue response of the cell.

A high barrier in the conduction band due to unfavorable band line-up or interface charge at the buffer/TCO junction may impede the majority carrier transport at this nn-junction. There are no indications for a significant barrier in standard cells but it has been made responsible for the poor performance of certain cells with alternative Cd-free buffer layers [9].

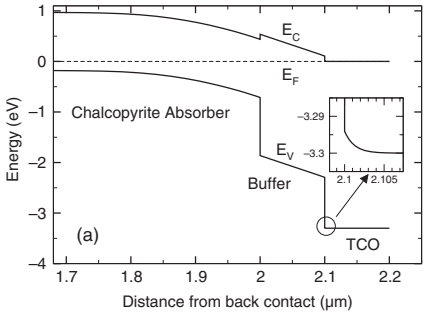

(a) Lightly doped buffer, no interface charge. The field zone extends through the buffer and into the TCO

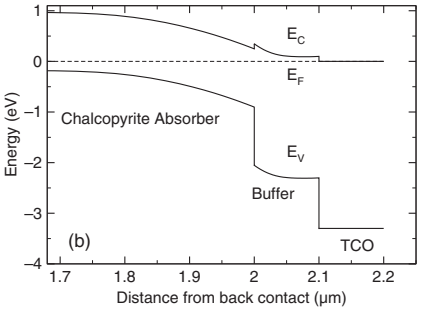

(b) Higher doping in the buffer layer. The field zone is limited to absorber and buffer

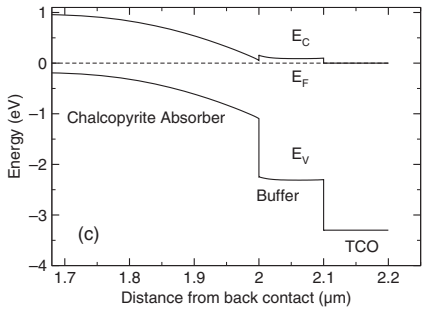

(c) Positive interface charge causes inversion of the absorber surface

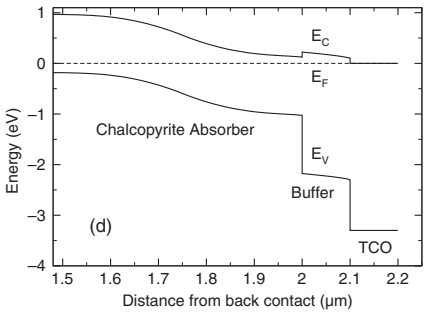

(d) Buried junction. The field zone is limited to the absorber

Fig. 9.3. Band diagrams of chalcopyrite/buffer/TCO heterojunctions illustrating the influence of buffer doping and interface charge

9.1.1 Why Use an Undoped ZnO Layer?

In the standard configuration, the ZnO film next to the CdS is sputtered from an undoped target or prepared by MOCVD without a dopant gas. It may also be sputtered from the same doped ZnO target that is used for the deposition of the conductive layer but with additional oxygen in the working gas. This film is commonly referred to as i-ZnO, which may be misleading because native defects cause a fairly high carrier density. Nevertheless, in view of the considerations made in the previous paragraph, depositing an i-ZnO film onto the CdS appears to be counter-productive. In addition, using undoped as well as doped targets increases production cost, in particular because the undoped ceramic target requires RF-sputtering. Ruckh et al. [10] have varied the thickness of the sputtered i-ZnO layer between 0 and 250 nm and have found no influence on open-circuit voltage and fill-factor of efficient lab-scale cells. The influence of sputtering parameters such as total pressure, argon and oxygen flow was also not significant. The authors

conclude that the i-ZnO does not at all participate in junction formation. The only effect noted was a higher stability at 200°C in air, i.e., a certain encapsulation or diffusion-barrier function of the i-ZnO layer. Similar experiments carried out by Kessler et al. confirm that high efficiencies can be achieved when omitting the undoped ZnO film [11], but presumably only if the CdS buffer is sufficiently thick [12]. Kessler et al. also report a better stability of cells with the undoped ZnO in accelerated ageing (damp heat test), which agrees with the encapsulation effect found by Ruckh et al. Finally, Ramanathan et al. report identical parameters of high efficiency cells with and without i-ZnO, even for the case of thin CdS buffers [13]. The stability was not assessed.

In spite of the described findings it is generally believed that – at least on module level – reproducibility and production-yield profit from inclusion of i-ZnO. It is obvious that the influence of localized flaws in the absorber film, such as pin-holes, is more severe if those are directly in contact with the highly doped contact layer [14]. Similarly, if the device properties are slightly inhomogeneous on a microscopic scale, the i-ZnO may be beneficial in terms of performance. Such inhomogeneities could be caused, e.g., by lateral bandgap fluctuations in the absorber film. In this case, the optimum resistivity of the i-ZnO will depend on the amount of fluctuations present [15].

9.2 Transparent Front Contact

While the ZnO double-layer may play a certain role in establishing the heterojunction, its major function is the lateral current transport to the contacts and the transmission of solar radiation into the absorber, i.e., acting as a transparent front contact. Unfortunately, high transparency and lowest sheet resistance are mutually exclusive ZnO properties. A given ZnO preparation process is therefore best described by plotting the achievable photocurrent vs. sheet resistance (Fig. 9.4). Transparency and resistance can be combined to give a figure of merit describing the performance of a ZnO film [16].

Small and medium area chalcopyrite solar cells are prepared for lab-scale testing and some special applications. Here the current collection is typically assisted by a metal grid deposited on top of the ZnO film, which relaxes the requirements for ZnO conductance. Depending on the spacing of the grid fingers, the ZnO can be fairly thin ($<0.5\,\mu m$), which is beneficial in terms of optical losses (see below). General experience shows that nickel makes a good and stable ohmic contact to highly doped ZnO. Additional metals such as aluminum are often used on top of a thin nickel film to reduce the grid resistance. However, large area modules are generally scribed into multiple cells which are monolithically connected in series and do not use a metal grid.

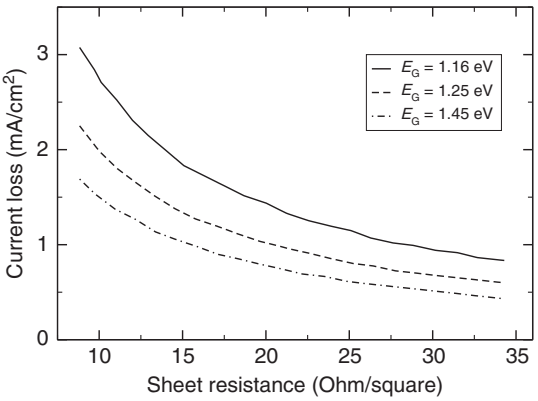

Fig. 9.4. Typical loss of current density as a function of ZnO sheet resistance calculated for three values of the absorber bandgap (assuming air mass 1.5 illumination, redrawn with permission from [12])

9.2.1 Monolithic Integration

The connection is made from the molybdenum back contact to the ZnO during ZnO deposition (Fig. 9.5). The common scheme requires three patterning steps: an isolation scribe in the molybdenum back contact (P1), an interconnect scribe of the absorber to create a gap, which is later filled by ZnO (P2), and an isolation scribe of the complete cell structure down to the molybdenum (P3). While the preferred tool for P1 patterning is a pulsed Nd-YAG laser, photo lithographic patterning is also possible. After laser patterning the substrate is subject to wet cleaning with rotating brushes to remove loose particles. P2 and P3 patterning are carried out by mechanical scribing. Appropriate tools must be used in order to avoid damaging the underlying molybdenum film. P2 patterning can be carried out before or after deposition of the undoped ZnO layer, the latter method may give a better contact between ZnO and molybdenum in P2.

Optimizing the ZnO requires a balance between conductance, transparency, and manufacturing cost. The series resistance of the device must be minimized to achieve a high fill factor. It depends on carrier density and mobility in the ZnO, thickness of the ZnO film, spacing of interconnects (grid finger spacing in case of cells), and the contact resistance between molybdenum and ZnO (nickel and ZnO). Higher doping may result in reduced mobility and higher optical losses, in particular in the long wavelength region (free carrier absorption/reflection). Increased thickness also affects the transparency and increases deposition time and costs. On the other hand, higher ZnO sheet resistance requires reducing the interconnect or finger spacing which in turn results in losses of active area. A high mobility is desirable because it reduces the series resistance without adversely affecting other parameters

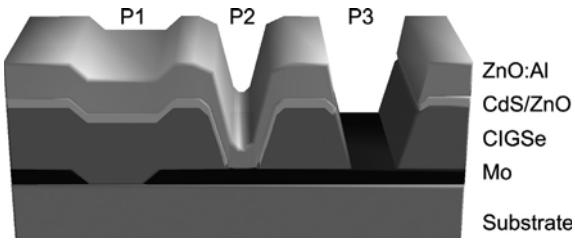

Fig. 9.5. Schematic cross-section of the cell interconnect in monolithic integration. This figure shows the variant where the P2 scribing is carried out after the deposition of the i-ZnO. Reprinted with permission from [1]

as long as the mobility can be achieved without costly modifications of the manufacturing process.

Depending on the composition of the absorber, typical photocurrent densities under full illumination range from 20 ($CuInS_2$ [19]) to 40 mA cm^{-2} (CISe [20]). Interconnect distance is 5–10 mm and causes a loss in active area of around 10%. The required ZnO thickness is around 1 µm. Nonideal ZnO transparency, series resistance, and loss in active area will cause an overall loss in module efficiency of about two percentage points compared to small area test cells prepared from the same materials. Results of a detailed calculation based on measured ZnO properties and carried out for different photocurrent densities (chalcopyrite absorber bandgap) can be found in [12]. They show a clear advantage of wide gap absorbers in terms of module efficiency. A computer simulation has been made available to optimize the module patterning for a given set of film properties [21]. Figure 9.6 shows data calculated by Wennerberg [17] using this program. Required input data are the ZnO sheet resistance and weighted optical transparency for varied thickness (in analogy to Fig. 9.4) as well as cell and interconnect properties. The data used here may be considered representative of the properties achievable in today's pilot production of evaporated CIGSe absorbers and of ZnO films sputtered from a ceramic target. Experimental verification can be carried out using a straightforward method described by Klaer et al. [18]. Results for $CuInS_2$-based test structures are shown in Fig. 9.7.

Given the current development status of ZnO thin films, a metal grid will result in higher cell or module [22] efficiency because the grid shading losses can be over-compensated by improved ZnO transparency and lower series resistance. In spite of this, grids are not used in commercial production of modules, presumably due to prohibitive cost, added complexity, and aesthetical reasons.

The ZnO film plays an important role for module stability in accelerated lifetime testing under damp heat conditions, which forms a part of the

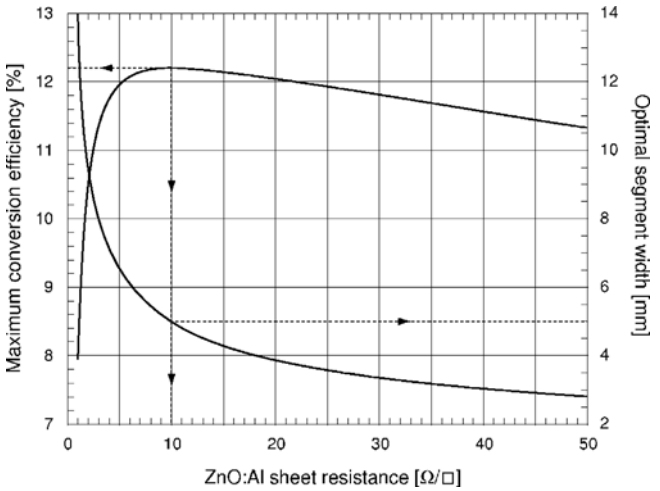

Fig. 9.6. Calculated optimum interconnect distance and resulting module efficiency as a function of ZnO sheet resistance. Calculations are based on the properties of a small area CIGSe-based cell with 14.4% efficiency. Reprinted with permission from [17]

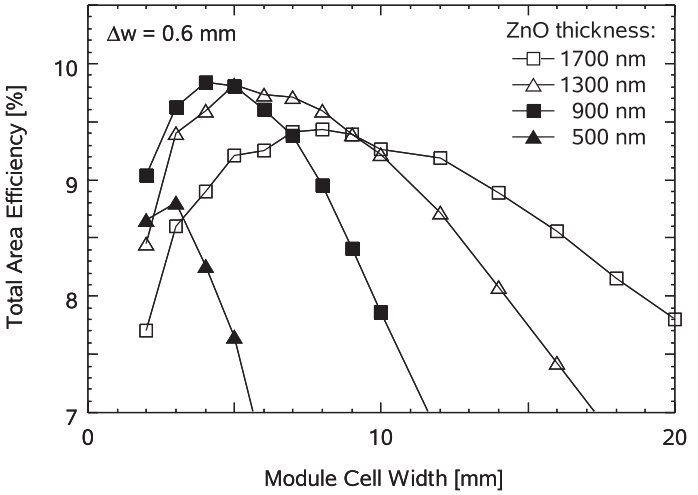

Fig. 9.7. $CuInS_2$-based module efficiency as a function of cell width for different ZnO layer thicknesses. The data are based on measurements of single module cells and calculated for a module having interconnects of 0.6 mm width. Reprinted with permission from [18]

EN/IEC 61646 certification. The lateral resistance tends to increase, giving rise to fill factor losses. It is therefore mandatory to optimize ZnO preparation not only with respect to the as-grown properties but also by taking into account the degradation in damp heat (see Sect. 9.4).

9.2.2 Optical Losses

Chalcopyrite-based devices generally show rather high photocurrent densities even without antireflective coating. Hence, apart from the issues described above, not much consideration has been given to optical losses caused by the ZnO films. The refractive indices within the device are not too far apart (ZnO $\approx$ 1.9, CdS $\approx$ 2.4, Absorber $\approx$ 2.9). Reflection at internal interfaces is therefore not severe. Interference fringes caused by the optical propagation in the window layer are sometimes noticeable in the spectral response of the device but only if the absorber is very smooth. Matching of refractive indices is also close to ideal for encapsulated devices. A simple single-layer antireflective coating deposited onto test structures without encapsulation will achieve maximum external quantum efficiencies of more than 95%. Light trapping does not play a significant role. The high optical absorption in the chalcopyrites together with an absorber thickness in the range of 2–3 µm guarantees that the light is completely absorbed in a single passage through the absorber. This is likely to change in the future when absorber layers will be made thinner to save on raw materials and production cost. New optical concepts for the chalcopyrite device are therefore being investigated, including reflecting back contacts [23] and ZnO front contacts optimized for light-trapping. The quest for record efficiencies in the lab as well as applications where efficiency is of paramount importance, e.g., applications in space are other motivations to optimize the optical design [24–26].

9.3 Manufacturing

Since in the chalcopyrite module the ZnO films are the last to be deposited, the processing must be compatible with the remainder of the cell structure. This implies in particular that substrate temperatures must be limited to 200–250°C [10] even though better ZnO properties could be achieved at higher deposition temperatures. Interdiffusion at the absorber/buffer interface has been made responsible for the instability [27] but it is believed that a detailed study using current state of the art material would be required to clarify this point.

It is important to realize that the actual film properties depend strongly on the substrate. A rough substrate (Fig. 9.8), such as absorber films from two-stage preparation [28], leads to a significant increase of the ZnO film resistance. The use of witness samples based on ideally smooth glass substrates may be misleading. The throughput needs to be fairly high. Actual and projected module production capacities are ranging from 1 to 50 MWp/a per facility, which roughly corresponds to cycle times from 30 to below 1 min. Deposition of ZnO contributes significantly to production costs [29]. In (pilot) production lines for chalcopyrite-based solar modules, ZnO is deposited by magnetron sputtering [29–31].

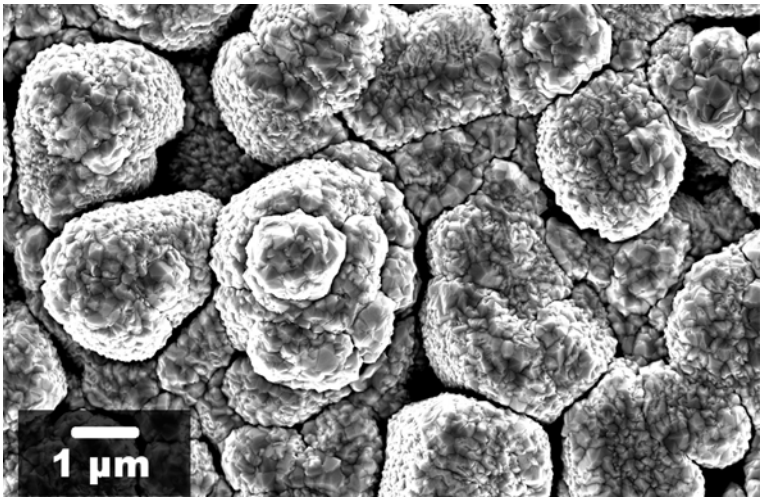

Fig. 9.8. Scanning electron micrograph of a ZnO:Al/ZnO/CdS/$CuInS_2$ solar cell. The larger structures correspond to the grains of the absorber layer

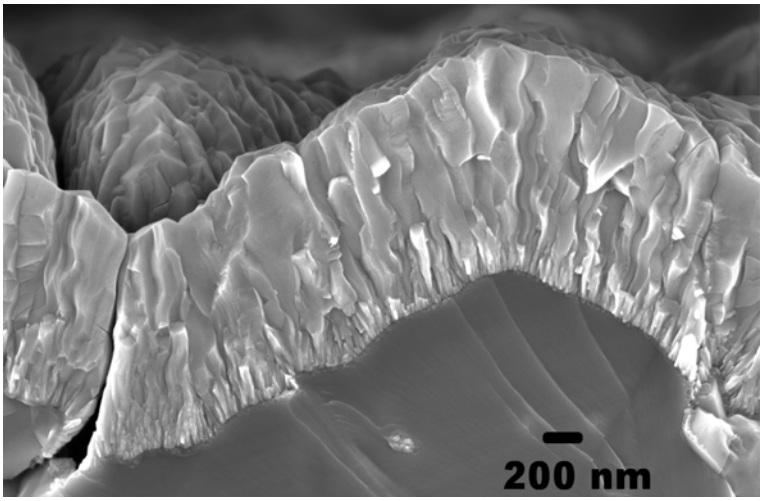

Fig. 9.9. Scanning electron micrograph of a ZnO:Al/ZnO/CdS/$CuInS_2$ solar cell (cross section)

9.3.1 Chemical Vapour Deposition[1]

The film is prepared by reacting diethylzinc (DEZn) with water vapour at the surface of the substrate heated to moderate temperatures, typically in the range of 150–200°C [32]. Inert gases are used to carry the reactants into the deposition chamber. Doping can be achieved by adding diborane to the atmosphere. Terzini et al. have compared the junction formation using sputtered and chemical vapour deposition (CVD) ZnO, in both cases without extrinsic doping, and have not identified significant differences [33]. CVD of ZnO has been used in previous pilot production lines with good results [34].

9.3.2 Sputtering

ZnO for cells and small modules can be prepared by RF-sputtering, which is known to yield good film properties [35]. Results of an optimization study can be found in [11]. Fine-tuning must be carried out using the actual absorber, buffer layers, metal grids, and antireflective coating in order to optimize the complete system. The NREL group uses a combination of a 90 nm undoped and a 120 nm doped film for their high efficiency devices [36]. The resistance is given as $60\,\Omega\,\mathrm{sq}^{-1}$ but it is not clear whether this is measured in the actual device or on witness samples.

For industrial production of large area modules, RF-sputtering of the doped ZnO is too slow and too expensive. RF-sputtering may still be used for deposition of the relatively thin undoped ZnO film. The thicker, highly doped film must be sputtered with DC or MF excitation of the plasma. DC sputtering from doped ceramic targets is feasible due to progress in target manufacturing and power supply technology (arc suppression). It is the preferred technology in pilot lines. Novel production methods have significantly reduced the high costs of ceramic targets. Further progress in target utilization may be possible by using rotating targets. It is conceivable that DC sputtering from ceramic targets will remain the preferred method when transitioning from pilot production to commercial production with higher capacity. Otherwise, reactive sputtering from metal targets is an alternative process promising high deposition rates and low cost.

Typical pilot line sputtering systems are in-line systems with dynamic deposition where the substrate passes one or more targets. The substrates are additionally heated in some but not in all systems. The systems are partly derived from those sold otherwise for ITO-deposition in flat panel display

[1] The CVD processing of ZnO for thin film solar cells is extensively described in Chap. 6. Details on CVD ZnO in Cu(In,Ga)Se_2 thin film solar cells can be found in Sects. 6.3.1.1 and 6.3.2.1.

manufacturing. There is no clear preference for vertical or horizontal configuration. Reasonable film properties, high throughput, and stable processes at low cost are obvious challenges to be met. In addition, ZnO deposited on chamber walls, shields, or even redeposited onto target areas outside the erosion zones exhibits particularly poor adhesion. ZnO flakes, particles, and dust may cause pin-holes in the module. Frequent cleaning of the deposition system may be required and limits its useful uptime.

9.3.2.1 DC Sputtering from Ceramic Targets

Results of a comprehensive study on DC sputtered ZnO for CIGSe-based modules can be found in [37]. Optical and electrical film properties were determined for varied target doping (ZnO:Al, ZnO:Ga) and sputtering conditions, in particular the oxygen flow. A normalized photocurrent was calculated from the measured transmission spectra using the spectral response of a highly efficient CIGSe solar cell. A model curve describing the normalized photo current as a function of ZnO sheet resistance was extrapolated from the experimental data and used as input for numerical calculations of module efficiency. It was concluded that – given the properties of the DC-sputtered ZnO – the optimal interconnect distance is 5 mm. An efficiency within 2% of the optimum was predicted for ZnO sheet resistance ranging from 7.5 to $20\,\Omega\,\mathrm{sq}^{-1}$. These values can be achieved with a target doping of 1.6–3.2% (metals ratio) and fine-tuned with the oxygen flow. Dynamic deposition rates of $80\,\mathrm{nm\,m\,min}^{-1}$ could be achieved. The authors point out the strong variations of the conductivity with minima directly opposite to the target erosion zones (race track) measured on test substrates deposited in static mode and conclude that this prevents achievement of optimum film properties in dynamic mode. It was found later that the conductivity profile under the target depends on the age of the target, i.e., the depth of the race track [38].

9.3.2.2 Reactive Sputtering

Reactive sputtering, i.e., sputtering from a metal rather than ceramic target is one of the options investigated for cost reductions. Already in 1996 it was reported that reactive DC sputtering can achieve the same cell efficiency as RF-sputtering from a ceramic target [10] even though the static deposition rate ($300\,\mathrm{nm\,min}^{-1}$) was ten times higher using the former method. The authors point out the importance of tight process control, in this case plasma emission monitoring (PEM), to obtain the required film properties at the low substrate temperature permitted by the chalcopyrite-based junction. Various problems concerning homogeneity, set point drift, and flaking have been encountered when reactive sputtering was evaluated in the Wuerth Solar pilot line [39] using a PEM controlled DC/DC dual magnetron process.

Nevertheless, efficiencies of more than 10% have been reported for full-size modules, only slightly lower than that of the standard modules prepared using a ceramic target. Sittinger et al. report on an MF-excited dual magnetron process using λ-sensors for oxygen partial pressure control. The process was originally developed for thin-film silicon modules where higher substrate temperatures can be used [40]. High efficiency as well as good stability of CIGSe-based mini-modules could be demonstrated after readjusting the deposition parameters [41].

9.4 Stability

Outdoor testing of chalcopyrite-based modules has generally demonstrated excellent stability [42, 43]. Owing to the increasing production volume there is a growing number of installations where the actual performance [44] and long-term stability can be assessed. Chalcopyrites do not suffer from any form of light-induced degradation. They are also known for their extraordinary radiation hardness and for their capability to passivate defects at comparably low temperatures [45].

Accelerated lifetime testing, especially the damp heat testing procedure (85°C, 85% humidity, 1 000 h), which forms a part of the EN/IEC 61646 certification, has, however, been cumbersome [46]. Partly, this is due to transient effects which occur during stress tests [47]. These can lead to an apparent degradation but the efficiency recovers after several days of light-soaking. As we will describe in the following sections, the exact causes for degradation are still under investigation; nevertheless, empirical optimization has achieved modules that have been independently certified [43, 47, 48].

ZnO serves different purposes in the chalcopyrite-based solar cells, hence, a degradation of ZnO properties in damp heat may affect the device performance in several ways. If the stability is examined using small individual cells with metal grid, the observed device degradation is mainly due to some deterioration of the heterojunction itself [49]. The stability of an interconnected module is in addition also affected by increasing ZnO sheet resistance and deteriorating interconnect properties and is therefore more severe [50]. Investigations aimed at identifying the basic degradation mechanisms are usually carried out by exposing *non-encapsulated* films and devices to the conditions according to IEC/EN 61646. It is often silently assumed that the degradation observed under these extremely harsh conditions is governed by the same physical and chemical effects as the small degradation, which is actually allowable for encapsulated modules passing the test (not more than 5% change in efficiency). Experimental results described by different authors are sometimes contradictory, which indicates that the fundamental mechanisms are not well understood.

9.4.1 Module Degradation

Accelerated ageing according to IEC/EN 61646 implies elevated temperature as well as high humidity. It has been reported that there is a module power loss already due to storing the module at the elevated temperature (dry heat) [47]. This power loss could be reversed by prolonged illumination (light-soaking), whereas the degradation caused by the humidity was irreversible. Other modules or test structures appear to be perfectly stable in dry heat and do not exhibit the reversible power loss [51].

A major degradation mechanism of modules is the decrease in fill factor. This is caused by an increase in the diode quality factor of the cells making up the module and by an increase in series resistance. The former is related more to the absorber and heterojunction properties and less to the ZnO properties. The series resistance increases because the conductivity of the ZnO drops and because the interconnects are deteriorating. Wennerberg et al. have assessed the individual contributions to increased series resistance [50]. Klaer et al. [52, 53] have described a transmission-line test structure that allows to separate the contributions of contact and sheet resistance, respectively. The test structure is prepared by the same scribing techniques as those used in module manufacturing.

9.4.1.1 Interconnect Corrosion

Increased series resistance due to interconnect corrosion has two possible origins: degradation of the Mo/ZnO contact (P2 interconnect via) and corrosion of the molybdenum which is exposed to the atmosphere in the P3 scribe-line. Bare molybdenum films on glass corrode rapidly in damp heat and partially form a transparent oxide. Nevertheless, corrosion of the molybdenum in P3 does not seem to contribute significantly to the module degradation until the molybdenum in the scribe has oxidized completely, the interconnect is broken, and the module efficiency is practically zero [54]. It has been reported that molybdenum corrosion occurs faster when the molybdenum film is mechanically stressed [55]. Nevertheless, total breakdown of the interconnect should happen only under unrealistically extreme conditions.

Wennerberg et al. argue that degradation of the Mo/ZnO contact resistance (P2 interconnect via) is to blame for most of the increased resistance [50]. They find that the contact resistance increases by almost two orders of magnitude, whereas the ZnO sheet resistance increases by only 50% after 500 h. Using locally resolved X-ray emission spectroscopy, Fischer et al. have found indications that, in P2, the ZnO reacts with molybdenum-chalcogenides during damp heat. This may explain contact degradation by formation of compounds with low conductivity [56] (molybdenum-chalcogenides can form during absorber preparation). Klaer et al. confirm a certain degradation of the interconnect but conclude that the increase in ZnO sheet resistance is more significant [52, 53]. They find a better stability of the interconnect when

the P2 scribe is carried out after the deposition of i-ZnO and before deposition of n^+-ZnO. This process sequence results in an Mo/n^+-ZnO via rather than an Mo/i-ZnO/n^+-ZnO interconnect. The disadvantage of this sequence lies in higher manufacturing cost due to the necessity to interrupt the ZnO deposition and break the vacuum for the patterning step.

9.4.1.2 ZnO Degradation

As described above, there is no general consensus in literature concerning the relative contributions of contact corrosion and increasing ZnO sheet resistance to increased module series resistance. However, experiments carried out within a recent joint research project in Germany suggest that degradation of the ZnO sheet resistance may indeed be the principle cause of damp heat instability. Large area absorbers provided by Wuerth Solar were diced into many nominally identical samples and coated with likewise nominally identical CdS buffer layers. ZnO films were then deposited onto these samples by several project participants using a range of different sputtering systems and parameters. The ZnO sheet resistance was measured directly on these substrates before and after different periods of damp heat ageing (without any encapsulation). All samples showed a sheet resistance increasing systematically with ageing. There was also a clear correlation between the increased ZnO sheet resistance and degradation of module test structures prepared under the same conditions. However, the described effects varied strongly among the different ZnO layers [38, 41]. In general, conditions which favor the growth of dense films and good step coverage (RF excitation, low pressure, high temperature, moving substrate) tend to yield better stability.

In addition to the deposition conditions, the ZnO microstructure is also heavily influenced by the substrate. In view of the findings described above it is not surprising that ZnO films deposited onto smooth substrates are much more stable than those deposited onto rough substrates. This is best illustrated by experiments [57] where polished and texture-etched silicon wafers were used as model substrates (Figs. 9.10 and 9.11).

The free carrier optical reflection of test modules before and after damp heat indicates that the effective carrier density is not much affected [58]. Hence, the degradation of the ZnO sheet resistance is probably more of a carrier transport problem. It is, at present, unclear where electron barriers are located. They may be present at the grain boundaries in general [59]. In this case, the disturbances of the ZnO microstructure (induced by the substrate but also depending on preparation parameters) are only harmful because they allow a faster penetration of the humidity into the film. On the other hand, the disturbed regions may themselves be highly resistive after damp heat exposure, which forces the current to percolate around these areas.

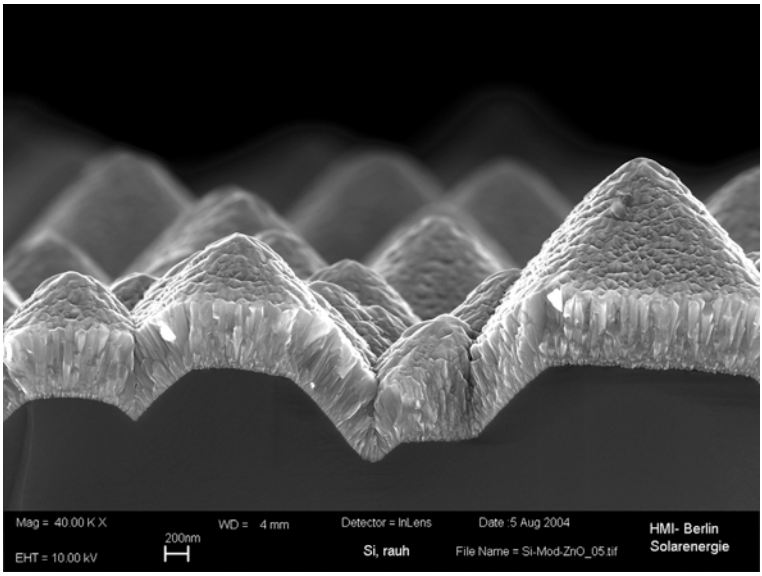

Fig. 9.10. Scanning electron micrograph of a ZnO thin film on a texture-etched silicon substrate. The ZnO microstructure is disturbed where one pyramid of the substrate borders the next pyramid

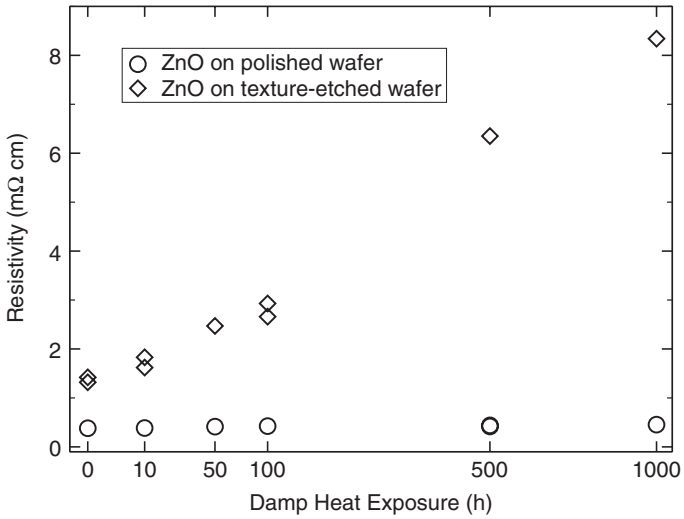

Fig. 9.11. Resistivity of ZnO thin films as a function of damp heat exposure (no encapsulation)

9.5 Nonconventional and Novel Applications

9.5.1 Direct ZnO/Chalcopyrite Junctions

The standard device comprises a thin CdS buffer layer as described above. It is believed that market acceptance of chalcopyrite-based photovoltaics could be improved by introducing a Cd-free buffer layer. There may also be cost benefits in view of the cost associated with (occupational) safety, handling of toxic waste in production, and recycling of modules at their end of life. Research has identified Cd-free materials well suited for alternative buffer layers. They can be deposited by CBD in analogy to the standard CdS buffer layers or by other processes. In particular, dry processes are attractive because they offer a better compatibility with the other process steps used for the remainder of the module. Ultimately, the best solution would be to omit the buffer layer altogether in favor of a direct chalcopyrite-sputtered/MOCVD ZnO junction. Here we will limit the discussion to the state of these latter direct junctions and to ZnO-based buffer layers (Table 9.1). Results achieved with other materials can be found in the literature [67, 68].

It had been assumed originally that CdS is required for lattice matching and conduction band alignment. It is therefore somewhat surprising that it is in effect possible to use a ZnO buffer layer. As we have shown elsewhere, however, interface recombination can be suppressed to an insignificant level not only by reducing the interface recombination velocity (which would require lattice matching) but also by reducing the number of carriers available for recombination [5]. In consequence, an efficient device can be expected whenever we succeed in positioning the Fermi-level close to the conduction band at the hetero-interface. In general this can be achieved by a suitable defect distribution (shallow donors) and band alignment at the interface. Judging from the experimental approaches that have been successful in terms of device performance, wet chemical surface conditioning, and mixing ZnO with other compounds seem to play an important role in establishing

Table 9.1. Performance of ZnO/chalcopyrite solar cells without buffer layer

Reference	Technology	Efficiency(%)
Negami et al. [60]	Evaporation of Zn, sputtering of (Zn,Mg)O	16.2
Ramanathan et al. [61]	Partial electrolyte, sputtering	15.3
Bär et al. [62]	Partial electrolyte, ion layer gas reaction	15
Glatzel et al. [63]	Sputtering of (Zn,Mg)O	12.5
Olsen et al. [64]	Chemical vapour deposition	12
Strohm et al. [65]	Sputtering of (Zn,Mg)O	11.5
Lincot et al. [66]	Electrodeposition ($2\,mm^2$)	9.2

Table 9.2. Superstrate cells

Reference	TCO	Buffer	Absorber	Efficiency
Klenk et al. [69]	ZnO	None	$CuGaSe_2$	$V_{oc} > 800\,mV$
Yoshida et al. [70]	ITO	CdS	$CuInSe_2$	6.6%
Negami et al. [71]	ZnO	CdS	$CuInSe_2$	6.7%
Haug et al. [72]	ZnO	None	$Cu(In,Ga)Se_2$	11.2%
Nakada et al. [73]	ZnO	None	$Cu(In,Ga)Se_2$	12.8%

the described criteria. It is interesting that in the reversed superstrate structure (see below) direct junctions perform better than those with a buffer layer.

9.5.2 Superstrates

The conventional cell structure is supported by a substrate onto which the layers are deposited with the doped ZnO being the final layer. Reversing the whole structure by depositing first the ZnO followed by the remaining layers results in a structure where the light enters the cell through the superstrate (Fig. 9.12). This concept has some potential advantages:

- The ZnO can be deposited at high temperature, resulting in improved optical and electrical properties and stability. Presumably its thickness could be reduced resulting in lower cost.
- Since the light enters through the superstrate the encapsulation does not have to be transparent. Nontransparent foils could be more cost effective than glass and reduce the module weight.
- Mechanically stacked tandem structures could be realized in a straightforward manner by fabricating one part in substrate and the other in superstrate configuration and then laminating them together.

However, preparing a blocking contact in superstrate structure has been difficult. Only small area cells have been demonstrated so far and even those show limited performance (Table 9.2). To achieve optimum properties, the absorber layer must be prepared at temperatures of about 500°C, which implies that interdiffusion is significant and may lead to a deterioration of junction and absorber bulk properties. It is interesting to note that approaches not using buffer layers have resulted in higher efficiency than those using CdS buffers prepared by various methods.

9.5.3 Transparent Back Contact

All ZnO/(buffer)/chalcopyrite junctions described so far in this contribution are blocking junctions as may be expected from the conductivity type

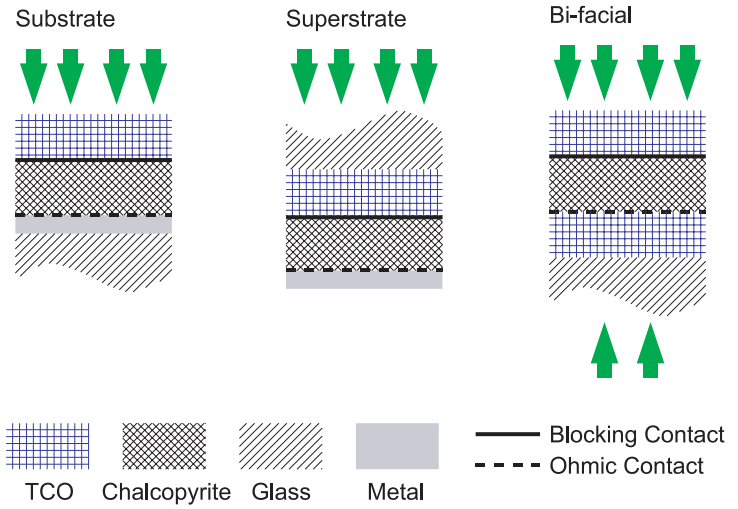

Fig. 9.12. Schematic cross-sectional views of chalcopyrite solar cell configurations. Reprinted with permission from [1]

of ZnO (n-type) and chalcopyrite (p-type), respectively. However, in the absence of technically viable p-type TCOs there is a certain interest also in making ohmic (nonblocking) contacts to n-type TCO. Experimental results demonstrate that this is feasible. Replacing the molybdenum film of the conventional structure by a TCO film then results in a cell with a transparent back contact. Such a structure may be useful in implementing bifacial or tandem cells, or semi-transparent modules [73] (Fig. 9.12). Again, the high substrate temperature necessary for absorber preparation is problematic and may lead to a deterioration of transparency and conductivity of the TCO film. In addition the absorber may be poisoned by elements diffusing from the TCO film. In many studies ZnO was found to be less suitable than other materials (such as SnO_2 or ITO) for this particular application [73, 74]. It has been demonstrated, however, that a very thin molybdenum film deposited onto the ZnO significantly improves the performance of devices with ZnO back contact. It is believed that the molybdenum is converted to $MoSe_2$ (a semiconductor with $E_g = 1.2\,\text{eV}$) during deposition of the absorber [75].

The efficiency for backside illumination (bi-facial cells) is limited because the carriers are generated outside the field zone in proximity to the poorly passivated contact (poor blue response). Further optimization of absorber thickness, diffusion length, and contact passivation appears to be feasible.

The efficiency of wide gap chalcopyrite cells, even on standard nontransparent substrate is too low for the realization of tandem cell. Using a TCO back contact reduces the efficiency even further. Establishing a high transparency is also not straightforward. Nevertheless, the potential of tandem

cells is reflected in wide-spread research activities. Preliminary prototypes are described in literature [76, 77].

The standard molybdenum contact is characterized by low optical reflection, which becomes relevant in efforts to reduce the absorber thickness (light trapping). A study of other metals has not identified clearly promising alternatives [78]. Hence, an ohmic contact between TCO and chalcopyrite with good electrical and optical properties could also be useful in developing a cell with a high reflectivity metal/TCO back contact.

References

1. J. Poortmans, V. Archipov, "Thin Film Solar Cells", Wiley & Sons, 2006
2. K. Ramanathan, M.A. Contreras, C.L. Perkins, S. Asher, F.S. Hasoon, J. Keane, D. Young, M. Romero, W. Metzger, R. Noufi, J. Ward, A. Duda, Prog. Photovolt: Res. Appl. **11**, 225 (2003)
3. S. Wagner, J.L. Shay, P. Migliorato, H.M. Kasper, Appl. Phys. Lett. **25**, 434 (1974)
4. R.R. Potter, C. Eberspacher, L.B. Fabick, in *Proceedings of the 18th IEEE Photovoltaic Specialists Conference*, 1985, p. 1659
5. R. Klenk, Thin Solid Films **387**, 135 (2001)
6. D. Schmid, M. Ruckh, F. Grunwald, H.W. Schock, J. Appl. Phys. **73**, 2902 (1993)
7. T. Wada, S. Hayashi, Y. Hashimoto, S. Nishiwaki, T. Sato, T. Negami, M. Nishitani, in *Proceedings of the 2nd World Conference Photovoltaic Solar Energy Conversion*, 1998, p. 403
8. K. Ramanathan, R. Noufi, J. Granata, J. Webb, J. Keane, Solar Energy Mater. & Sol Cells **55**, 330 (1998)
9. Q. Nguyen, K. Orgassa, I. Koetschau, U. Rau, H.W. Schock, Thin Solid Films **431–432**, 330 (2003)
10. M. Ruckh, D. Hariskos, U. Rühle, H.W. Schock, R. Menner, B. Dimmler, in *Proceedings of the 25th IEEE Photovoltaic Specialists Conference*, 1996, p. 825
11. J. Kessler, J. Norling, O. Lundberg, J. Wennerberg, L. Stolt, in *Proceedings of the 16th European Photovoltaic Solar Energy Conference*, 2000, p. 775
12. J. Kessler, S. Wiedeman, L. Russell, J. Fogleboch, S. Skibo, R. Arya, D. Carlson, in *Proceedings of the 25th IEEE Photovoltaic Specialists Conference*, 1996, p. 885
13. K. Ramanathan, J. Keane, R. Noufi, in *Proceedings of the 31st IEEE Photovoltaic Specialists Conference*, 2005, p. 195
14. U. Rau, M. Schmidt, Thin Solid Films **387**, 141 (2001)
15. U. Rau, P.O. Grabitz, J.H. Werner, Appl. Phys. Lett. **85**, 6010 (2004)
16. G. Haacke, Appl. Phys. Lett. **47**, 4086 (1976)
17. J. Wennerberg, *Design and Stability of Cu(In,Ga)Se_2-Based Solar Cell Modules*, Ph.D. Thesis, Uppsala University, 2002
18. J. Klaer, I. Luck, A. Boden, R. Klenk, I. Gavilanes-Perez, R. Scheer, Thin Solid Films **431–432**, 534 (2003)
19. R. Klenk, J. Klaer, R. Scheer, M.C. Lux-Steiner, I. Luck, N. Meyer, U. Rühle, Thin Solid Films **480–481**, 509 (2005)

20. J. AbuShama, R. Noufi, S. Johnston, S. Ward, X. Wu, in *Proceedings of the 31st IEEE Photovoltaic Specialists Conference*, 2005, p. 299
21. M. Burgelman, A. Niemegeers, Solar Energy Mater. & Sol Cells **51**, 129 (1998)
22. J. Kessler, J. Wennerberg, M. Bodegård, L. Stolt, Solar Energy Mater. & Sol Cells **75**, 35 (75)
23. K. Orgassa, H.W. Schock, J.H. Werner, Thin Solid Films **431–432**, 387 (2003)
24. K. Orgassa, Q. Nguyen, I.M. Kötschau, U. Rau, H.W. Schock, J.H. Werner, in *Proceedings of the 17th European Photovoltaic Solar Energy Conference*, 2001, p. 391
25. K. Orgassa, U. Rau, Q. Nguyen, H.W. Schock, J.H. Werner, Prog. Photovolt: Res. Appl. **10**, 457 (2002)
26. C.A. Kaufmann, A. Neisser, R. Klenk, R. Scheer, H.W. Schock, Mater. Res. Soc. Symp. Proc. **865**, F7.5.1 (2005)
27. L.L. Kazmerski, O. Jamjoum, P.J. Ireland, R.A. Mickelsen, W.S. Chen, J. Vac. Sci. Technol. **21**, 486 (1982)
28. B.M. Basol, V.J. Kapur, in *Proceedings of the 21st IEEE Photovoltaic Specialists Conference*, 1990, p. 546
29. N. Meyer, I. Luck, U. Rühle, J. Klaer, R. Klenk, M.C. Lux-Steiner, R. Scheer, in *Proceedings of the 19th European Photovoltaic Solar Energy Conference*, 2004, p. 1698
30. B. Dimmler, M. Powalla, R. Schaeffler, in *Proceedings of the 31st IEEE Photovoltaic Specialists Conference*, 2005, p. 189
31. M. Oertel, B. Dimmler, in *Proceedings of the Workshop TCO für Dünnschichtsolarzellen und andere Anwendungen III*, 2005, p. 61
32. P.S. Vijayakumar, K.A. Blaker, R.D. Wieting, B. Wong, A.T. Halani, U.S. Patent 4,751,149, 1988
33. E. Terzini, A. Antonaia, P. Thilakan, S. Aprea, I. Luck, in *Proceedings of the 16th European Photovoltaic Solar Energy Conference*, 2000, p. 706
34. R.D. Wieting, in *Proceedings of the 29th IEEE Photovoltaic Specialists Conference*, 2002, p. 478
35. R.H. Mauch, J. Hedström, D. Lincot, M. Ruckh, J. Kessler, R. Klinger, L. Stolt, J. Vedel, H.W. Schock, in *Proceedings of the 22nd IEEE Photovoltaic Specialists Conference*, 1991, p. 898
36. K. Ramanathan, J.C. Keane, B. To, R.G. Dhere, R. Noufi, in *Proceedings of the 20th European Photovoltaic Solar Energy Conference*, 2005, p. 1695
37. R. Menner, R. Schäffler, B. Sprecher, B. Dimmler, in *Proceedings of the 2nd World Conference on Photovoltaic Solar Energy Conversion*, 1998, p. 1161
38. R. Menner, M. Powalla, in *Proceedings of the Workshop TCO für Dünnschichtsolarzellen und andere Anwendungen III*, 2005, p. 71
39. R. Menner, M. Oertel, M. Powalla, M. Dimer, S. Rehn, J. Strümpfel, B. Dimmler, in *Proceedings of the 19th European Photovoltaic Solar Energy Conference*, 2004, p. 1694
40. V. Sittinger, F. Ruske, W. Werner, S. B, B. Rech, J. Hüpkes, G. Schöpe, H. Stiebig, Thin Solid Films **496**, 16 (2006)
41. V. Sittinger, F. Ruske, W. Werner, B. Szyszka, R. Menner, M. Powalla, B. Dimmler, in *Proceedings of the 21st European Photovoltaic Solar Energy Conference*, 2006
42. L. Mrig, S. Rummel, in *Proceedings of the 21st IEEE Photovoltaic Specialists Conference*, 1990, p. 1038

43. M. Powalla, B. Dimmler, R. Schäffler, G. Voorwinden, U. Stein, H.D. Mohring, F. Kessler, D. Hariskos, in *Proceedings of the 19th European Photovoltaic Solar Energy Conference*, 1663, p. 1663
44. H.D. Mohring, D. Stellbogen, R. Schäffler, S. Oelting, R. Gegenwart, P. Konttinen, T. Carlsson, M. Cendagorta, W. Herrmann, in *Proceedings of the 19th European Photovoltaic Solar Energy Conference*, 2004, p. 2098
45. A. Jasenek, A. Boden, K. Weinert, M.R. Balboul, H.W. Schock, U. Rau, Mater. Res. Soc. Symp. Proc. **668**, H3.2.1 (2001)
46. J. Malmström, J. Wennerberg, L. Stolt, Thin Solid Films **431–432**, 436 (2003)
47. F. Karg, H. Calwer, J. Rimmasch, V. Probst, W. Riedl, W. Stetter, H. Vogt, M. Lampert, in *Proceedings of the 11th International Conference on Ternary and Multinary Compounds*, 1998, p. 909
48. J. Palm, V. Probst, W. Stetter, R. Toelle, S. Visbeck, H. Calwer, T. Niesen, H. Vogt, O. Hernandez, M. Wendl, F.H. Karg, Thin Solid Films **451–452**, 544 (2004)
49. J. Wennerberg, J. Kessler, M. Bodegård, L. Stolt, in *Proceedings of the 2nd World Conference on Photovoltaic Solar Energy Conversion*, 1998, p. 1161
50. J. Wennerberg, J. Kessler, L. Stolt, in *Proceedings of the 16th European Photovoltaic Solar Energy Conference*, 2000, p. 309
51. R. Scheer, R. Klenk, J. Klaer, I. Luck, Solar Energy **77**, 777 (2004)
52. J. Klaer, R. Scheer, R. Klenk, A. Boden, C. Köble, in *Proceedings of the 19th European Photovoltaic Solar Energy Conference*, 2004, p. 1847
53. J. Klaer, R. Klenk, A. Boden, A. Neisser, C. Kaufmann, R. Scheer, H.W. Schock, in *Proceedings of the 31st IEEE Photovoltaic Specialists Conference*, 2005, p. 336
54. M. Powalla, B. Dimmler, Solar Energy Mater. & Sol Cells **67**, 337 (2001)
55. J. Klaer, R. Klenk, C. Köble, A. Boden, R. Scheer, H.W. Schock, in *Proceedings of the 20th European Photovoltaic Solar Energy Conference*, 2005, p. 1914
56. C.H. Fischer, M. Bär, T. Glatzel, I. Lauermann, M.C. Lux-Steiner, Solar Energy Mater. & Sol Cells **90**, 1471 (2006)
57. R. Klenk, M. Linke, H. Angermann, C. Kelch, M. Kirsch, J. Klaer, C. Köble, in *Proceedings of the Workshop TCO für Dünnschichtsolarzellen und andere Anwendungen III*, 2005, p. 79
58. C. Köble, R. Klenk (unpublished results)
59. J.Y.W. Seto, J. Appl. Phys. **46**, 5427 (1975)
60. T. Negami, T. Aoyagi, T. Satoh, S. Shimakawa, S. Hayashi, Y. Hashimoto, in *Proceedings of the 29th IEEE Photovoltaic Specialists Conference*, 2002, p. 656
61. K. Ramanathan, F.S. Hasoon, S. Smith, D.L. Young, M.A. Contreras, P.K. Johnson, A.O. Pudov, J.R. Sites, J. Phys. Chem. Solids **64**, 1495 (2003)
62. M. Bär, C.H. Fischer, H.J. Muffler, B. Leupolt, T.P. Niesen, F. Karg, M.C. Lux-Steiner, in *Proceedings of the 29th IEEE Photovoltaic Specialists Conference*, 2002, p. 636
63. T. Glatzel, H. Steigert, R. Klenk, M.C. Lux-Steiner, T.P. Niesen, S. Visbeck, in Technical Digest of the 14th International PVSEC, 2004, p. 27–5
64. L.C. Olsen, H. Aguilar, F.W. Addis, W. Lei, J. Li, in *Proceedings of the 25th IEEE Photovoltaic Specialists Conference*, 1996, p. 997
65. A. Strohm, T. Schlötzer, Q. Nguyen, K. Orgassa, H. Wiesner, H.W. Schock, in *Proceedings of the 19th European Photovoltaic Solar Energy Conference*, 2004, p. 1741

66. D. Lincot, B. Canava, S. Quenet, S. Peulon, in *Proceedings of the 14th European Photovoltaic Solar Energy Conference*, 1997, p. 2168
67. S. Siebentritt, Solar Energy **77**, 767 (2004)
68. N.A. Allsop, A. Schönmann, H.J. Muffler, M. Bär, M.C. Lux-Steiner, C.H. Fischer, Prog. Photovolt: Res. Appl. **13**, 607 (2005)
69. R. Klenk, R. Mauch, R. Schäffler, D. Schmid, in *Proceedings of the 22nd IEEE Photovoltaic Specialists Conference*, 1991
70. T. Yoshida, R.W. Birkmire, in *Proceedings of the 11th E.C. Photovoltaic Solar Energy Conference*, 1992, p. 811
71. T. Negami, M. Nishitani, M. Ikeda, T. Wada, Solar Energy Mater. & Sol Cells **35**, 215 (1994)
72. F.J. Haug, D. Rudmann, H. Zogg, A.N. Tiwari, Thin Solid Films **431–432**, 431 (2003)
73. T. Nakada, Y. Hirabayashi, T. Tokado, D. Ohmori, T. Mise, Solar Energy **77**, 739 (2004)
74. S. Bakehe, R. Klenk, M.C. Lux-Steiner, in *Proceedings of the 19th European Photovoltaic Solar Energy Conference*, 2004
75. P.J. Rostan, J. Mattheis, G. Bilger, U. Rau, J.H. Werner, Thin Solid Films **480–481**, 67 (2005)
76. S. Nishiwaki, S. Siebentritt, P. Walk, M.C. Lux-Steiner, Prog. Photovolt: Res. Appl. **11**, 243 (2003)
77. M. Symko-Davies, R. Noufi, in *Proceedings of the 20th European Photovoltaic Solar Energy Conference*, 2005, p. 26
78. K. Orgassa, H.W. Schock, J.H. Werner, Thin Solid Films **431–432**, 387 (2003)